

Maximum information states for coherent scattering measurements

Dorian Bouchet,^{1,*} Stefan Rotter,² and Allard P. Mosk¹

¹Debye Institute for Nanomaterials Science, Utrecht University,
P.O. Box 80000, 3508 TA Utrecht, the Netherlands

²Institute for Theoretical Physics, Vienna University of Technology (TU Wien), A-1040 Vienna, Austria

The use of coherent light for precision measurements has been a key driving force for numerous research directions, ranging from biomedical optics [1, 2] to semiconductor manufacturing [3]. Recent work demonstrates that the precision of such measurements can be significantly improved by tailoring the spatial profile of light fields used for estimating an observable system parameter [4–10]. These advances naturally raise the intriguing question of which states of light can provide the ultimate measurement precision [11] and of how such states can be identified in an experiment. Here, we introduce a general approach to determine optimal coherent states of light for estimating any given parameter, regardless of the complexity of the system. Our analysis reveals that the light fields delivering the ultimate measurement precision are eigenstates of a Hermitian operator which quantifies the Fisher information based on the system’s scattering matrix [12, 13]. To illustrate this concept, we experimentally show that these maximum information states probe the phase of an object that is hidden by a disordered medium with a precision improved by an order of magnitude as compared to unoptimized states. Our results enable precision measurements in arbitrarily complex systems, with promising perspectives for metrology and imaging applications [3, 14].

No physical observable can be estimated with absolute precision. Instead, the noise inherent in any measurement process sets a fundamental limit on the precision that a physical observable can be estimated with [11, 15]. Whenever light or other kinds of electromagnetic radiation are involved in a measurement, a necessary condition to reach this ultimate precision is to optimize the spatial distribution of the radiation field in the measured system [14]. To achieve this goal, a crucial task is to identify the spatial pattern that should be imprinted on the incoming field in order to get the maximum information out of it. First progress in this direction has recently been made using wavefront shaping techniques and metasurfaces to precisely estimate lateral displacements [4, 8], fluorophore positions [5, 6], spectral shifts [7] or phase variations [10].

A central challenge that remains unresolved, however, is to identify a unifying approach to reach the ultimate precision limit that is applicable even to complex scattering systems. Earlier work suggests that such an approach should be connected to the concept of Fisher information [5, 9, 11, 15], which quantifies the amount of information relevant to the estimation of a given parameter from measured data. However, for the generic case of a complex medium, the Fisher information is intrinsically linked to the microstructure of the medium [9], which is not only overwhelmingly complex in realistic systems but also typically unknown.

Here, we overcome this difficulty by expressing the Fisher information in terms of a system’s optical scattering matrix S , which is nowadays routinely accessible in experiments through interferometric far-field measure-

ments [12]. Based on this idea, we introduce and experimentally demonstrate an operational procedure to generate optimal coherent states of light for parameter estimation, which is completely general in terms of the observable one may be interested in. On the conceptual level, this approach reveals that, for a fully available scattering matrix, the maximum information states are also the optimal states for optical micro-manipulation [16, 17], thereby uncovering a fundamental relationship between information theory and measurement backaction.

To set up this approach we recall that a measurement scheme is optimal when the measurements, the estimation function, and the choice of the incident state are all optimal concurrently [11]. To realize this situation for coherent states of light, we start with a general model of scattering measurements on a complex medium parameterized by a scalar parameter θ (Fig. 1). This parameter can be a global parameter characterizing the entire scattering medium. It can also be a local parameter of limited spatial extent such as the phase shift induced by a small object hidden behind a scattering material, as in our experiment (Fig. 2). The medium is illuminated from the far field by an incident coherent state E^{in} , which can be modulated using wavefront shaping techniques [18]. Quadrature components of the resulting outgoing state E^{out} are then measured in the far field at N independent sampling points using a homodyne detection scheme. This scheme is known to operate at the optimal noise limit: for a strong reference beam, the variance of the measured quadrature components of the field is limited by Heisenberg’s uncertainty principle.

Noise fluctuations in the measured data fundamentally limit the achievable precision on the determination of θ . This limit is mathematically expressed by the Cramér–Rao inequality, which sets a lower bound on the variance

* d.f.bouchet@uu.nl

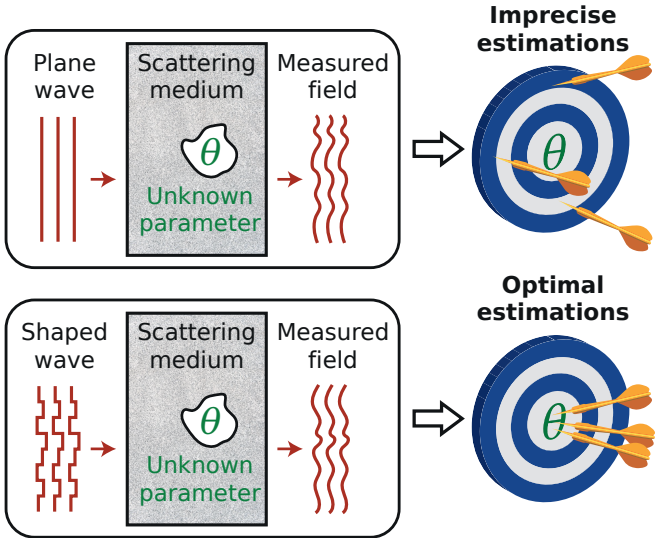


Fig. 1 | Principle of an optimal coherent scattering measurement. A scattering medium is characterized by an unknown parameter θ . This parameter is estimated by illuminating the medium with coherent light and by measuring the outgoing field state via a homodyne detection scheme. While plane-wave illumination may lead to imprecise estimations (top panel), the optimal incident state can be generated using waveform shaping techniques to perform optimal estimations (bottom panel).

of unbiased estimators of θ . In general, the Cramér-Rao bound is given by the reciprocal of the Fisher information $\mathcal{J}(\theta) = \mathbb{E}([\partial_\theta \ln p(X; \theta)]^2)$ where X is a N -dimensional random variable representing the data, $p(X; \theta)$ is a joint probability density function and \mathbb{E} denotes the expectation operator acting over noise fluctuations [15]. In the case of scattering measurements performed with a detection scheme optimized for the estimation of θ , a strong reference beam must be shaped so that its phase at the k -th sampling point is $\phi_k = \arg(\partial_\theta E_k^{\text{out}})$, where E_k^{out} denotes the outgoing field evaluated at the k -th sampling point (see Supplementary Information S1.1). Then, the statistical independence of the samples allow us to derive the following simplified expression for the Fisher information:

$$\mathcal{J}(\theta) = 4 \sum_{k=1}^N |\partial_\theta E_k^{\text{out}}|^2. \quad (1)$$

We can compare this expression of the classical Fisher information to its quantum counterpart, which sets a lower bound on the variance of unbiased estimators without any specification on the detection scheme [19]. Calculating the quantum Fisher information for coherent states and assuming statistical independence of the samples, the classical expression given by Eq. (1) is shown to reach the quantum limit (see Supplementary Information S1.2), thereby ensuring that the homodyne detection scheme considered here is optimal for the estimation of θ .

We now investigate the optimization of the incident state. An incident state E^{in} is optimal for the Fisher information it generates when the corresponding outgoing state E^{out} maximizes Eq. (1) for a given number of incident photons. In order to identify this state, the pivotal quantity is the scattering matrix S of the medium [13], which relates incoming and outgoing asymptotic states via $E^{\text{out}} = SE^{\text{in}}$. Using this relationship, the Fisher information can be written in the quadratic form $\mathcal{J}(\theta) = \langle E^{\text{in}} | F_\theta | E^{\text{in}} \rangle$, where we used bra-ket notations for the complex inner product. We designate the term F_θ in the center of this expression as the *Fisher information operator* that takes on the remarkably simple form (see Supplementary Information S1.3)

$$F_\theta = 4(\partial_\theta S)^\dagger \partial_\theta S, \quad (2)$$

where \dagger stands for the conjugate transpose. Since this operator F_θ is Hermitian already by construction, the incident state that maximizes the Fisher information is given by the eigenstate associated with the largest eigenvalue of F_θ . Furthermore, in the limit of small parameter variations, we obtained a closed-form expression of the minimum variance unbiased estimator (see Supplementary Information S1.4), which is the optimal estimation function. Importantly, the variance of this estimator always reaches the Cramér-Rao bound, which confirms that the Fisher information is the relevant quantity to compare the estimation precision achievable with different light states.

While only sub-parts of the S -matrix are usually measured in optics [12, 20], it is instructive to first discuss the canonical case of a complete and unitary S -matrix describing a scattering system without any loss or gain. In this case, we obtain the identity $F_\theta = 4Q_\theta^2$, where $Q_\theta = -iS^{-1}\partial_\theta S$ is the generalized Wigner-Smith operator. This operator was recently introduced to design optimal light fields for optical micro-manipulation in complex media [16, 17]. The simple relation between F_θ and Q_θ suggests a new interpretation of Q_θ as the operator representing the measurement backaction on the conjugate quantity to θ . Furthermore, the eigenstates of Q_θ (also called *principal modes*) have the remarkable property of being insensitive with respect to small variations in θ except for a global phase factor [21, 22]. Likewise, for a unitary S -matrix, the Fisher information of maximum information states is exclusively enclosed in variations of the global phase of the outgoing state, rather than in the state's intensity variations or speckle decorrelation.

In our experiment, we choose as the observable parameter θ that we aim to estimate the phase shift φ generated by a small cross (total length 48 μm) displayed by a spatial light modulator (SLM), as represented in Fig. 2. This target is hidden 1.2 mm behind a ground glass diffuser (scattering angle 15°). We illuminate this scattering medium using a continuous-wave laser (wavelength 532 nm) via a $\times 50$ objective (numerical aperture

0.6). The phase of the incident field is controlled using an SLM located in the conjugate plane of the surface of the diffuser. The horizontal component of the field is measured in reflection using an off-axis reference arm and a charge-coupled device (CCD) camera, which images the surface of the diffuser. Both quadrature components of the complex field are measured in a single shot using digital off-axis holography. Using a tilted beam instead of the optimally-shaped reference field does not impact the shape of the incident field optimized for the estimation of φ , but only leads to a reduction in the Fisher information by a factor of two (see Supplementary Information S2.1).

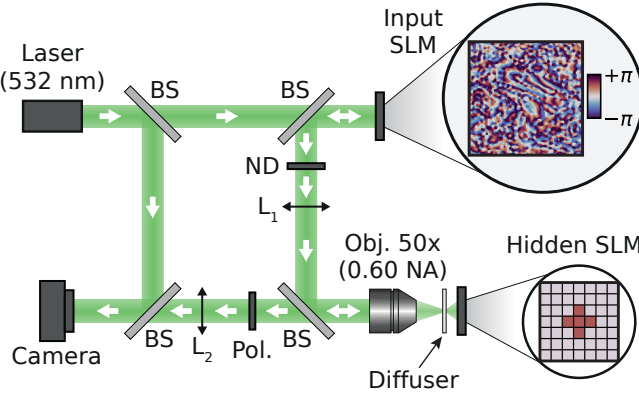


Fig. 2 | Optical setup for phase-contrast estimations. The phases on the input SLM are modulated to reproduce the maximum information state which reaches optimal sensitivity in its output with respect to phase variations induced by the cross on the hidden SLM. Neutral density filters are removed for reflection matrix measurements. BS, beamsplitter; ND, neutral density filters; Obj, objective; NA, numerical aperture; Pol, linear polarizer; L₁ and L₂, lenses with focal length 200 mm.

The acquisition procedure starts by measuring three reflection matrices for different values of φ . Reflection matrix measurements are performed by illuminating the medium with plane waves of different incident angles, and by sampling the measured field using a periodic lattice. The reflection matrix $r(\varphi_0)$ is measured by setting the phase shift induced by all pixels of the hidden SLM to zero. Two additional reflection matrices $r(\varphi_0 + \Delta\varphi)$ and $r(\varphi_0 - \Delta\varphi)$ are measured respectively by changing the phase shift induced by the whole target by $\pm\Delta\varphi$ where $\Delta\varphi = 0.54$ rad. The derivative of r with respect to φ is then estimated from the centered finite difference scheme $\partial_\varphi r \simeq [r(\varphi_0 + \Delta\varphi) - r(\varphi_0 - \Delta\varphi)]/(2\Delta\varphi)$. In this way, we characterize 2437 incident states and 2465 outgoing states (see Methods and Supplementary Information S3).

Even though the measured reflection matrix is large, it constitutes only a sub-part of the full S -matrix of the medium. This is not a limitation of our approach, which also applies to non-unitary and non-square matrices. Defining the operator $f_\varphi = (\partial_\varphi r)^\dagger \partial_\varphi r$, the eigen-

vector associated with the largest eigenvalue of f_φ is the optimal incident state based on the available knowledge. Injecting this state in the medium using the input SLM, we measured the spatial distributions of the outgoing signal intensity (Fig. 3a) and of the Fisher information per unit area (Fig. 3b), respectively normalized by the average signal intensity and by the average Fisher information per unit area under plane-wave illumination. For comparison purposes, we also measured the intensity (Fig. 3d) and Fisher information per unit area (Fig. 3e) for a plane wave. Averaging over the field of view, we observe a 300-fold enhancement of the Fisher information for the maximum information state, along with a 24-fold intensity enhancement. For the maximum information state, we also remark that the intensity and the Fisher information per unit area are correlated in their spatial profile. More precisely, the correlation between E^{out} and $\partial_\varphi E^{\text{out}}$ is characterized by a complex correlation coefficient of 0.96 i , which indicates that the information on φ is primarily enclosed in the phase of the outgoing state (see Supplementary Information S3.3). This feature reflects the invariance property of principal modes, which are invariant (to first order) in their output profile with respect to parameter variations except for a global phase shift [21, 22].

We also checked explicitly in which way the maximum information state is unique in terms of its near-field at the cross-shaped phase perturbation. To this end, we measured the Fisher information in the outgoing state for phase variations on each individual pixel on the hidden SLM. This is achieved by setting the phase shift induced by all pixels to zero, and by successively varying the phase shift induced by individual pixels sequentially instead of varying the phase shift induced by the cross-shaped target as a whole. We find that the maximum information state is primarily sensitive to the 5 pixels defining the cross (Fig. 3c), while the sensitivity of a plane wave is much lower and randomly spread over all considered pixels on the SLM (Fig. 3f). This observation confirms the specificity of maximum information states and their economical wave function design. We emphasize that optimal states are not conceived to reveal the shape of the target, but to estimate the phase shift it induces. This does not require the intensity to be uniformly distributed on the area defining the target, explaining why its shape is not always fully revealed (see also Extended Data Fig. 2 for measurements performed with a different object shape).

To show the remarkable advantages these features provide for measurements with very few photons where the estimation precision is limited by shot noise, we reduce the incident photon flux by placing a neutral density filter (fractional transmittance 8.3×10^{-7}) in the optical path. Under these conditions, illuminating the medium with a plane wave does not allow reliable estimations for the phase shift induced by target. This is confirmed by

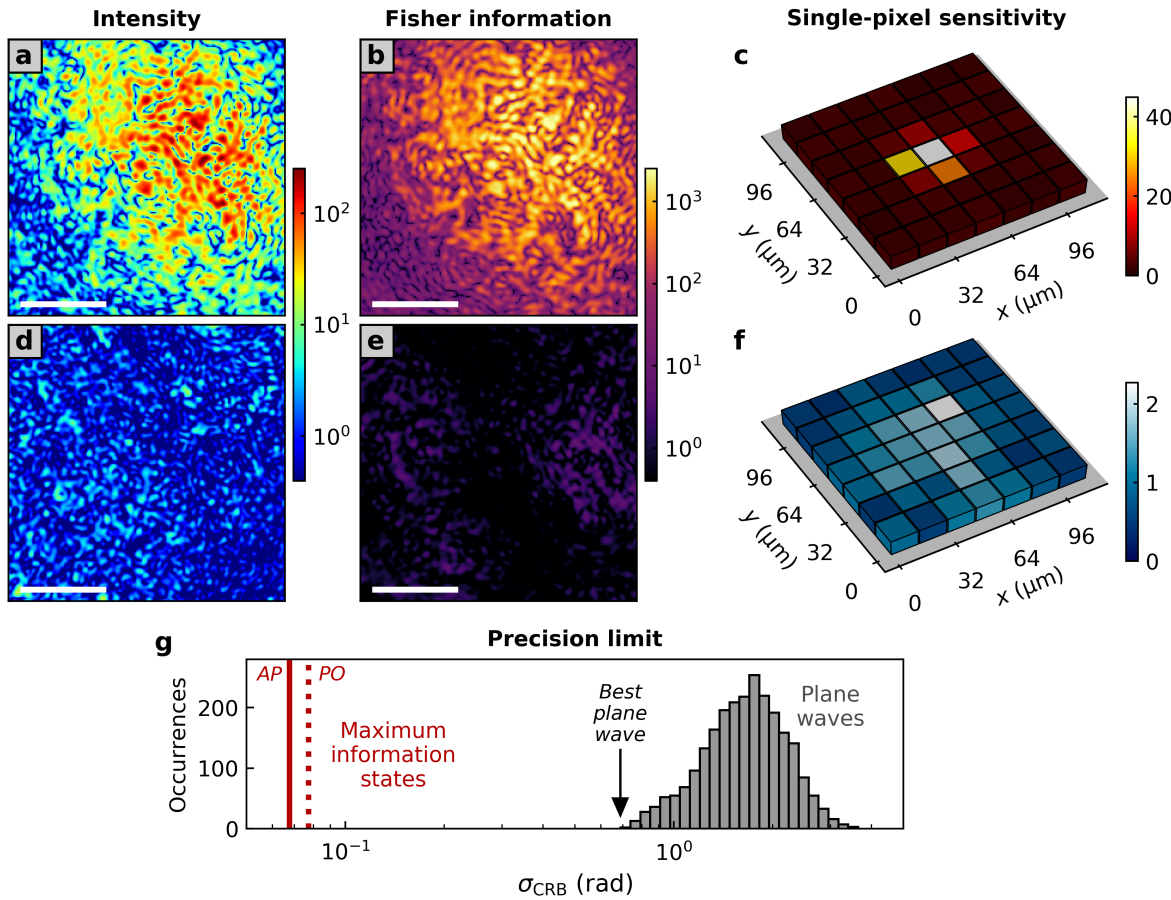


Fig. 3 | Examination of a maximum information state. **a, b**, Measured spatial distributions of the intensity and of the Fisher information per unit area for the optimal state, respectively normalized by the average signal intensity and by the average Fisher information per unit area under plane-wave illumination. **c**, Fisher information associated with each pixel in the target area of the hidden SLM for the optimal state, normalized by the average Fisher information under plane-wave illumination. A pixel is defined here as an ensemble of four physical pixels of the hidden SLM. **d–f**, Analogous to **a–c** for a plane wave, selected as the plane wave whose precision limit equals the median value observed under plane-wave illumination. **g**, Histogram of precision limits for the 2437 plane waves used to construct the reflection matrix. As compared to the best plane wave, the precision limit is improved by an order of magnitude with the maximum information states (AP, amplitude and phase modulation; PO, phase-only modulation). Scale bars in **a**, **b**, **d** and **e**, 10 μm .

calculating the precision limit σ_{CRB} for the 2437 plane waves used to construct the reflection matrix (see Supplementary Information S2). For these plane waves, the median of the distribution is 1.7 rad, with a minimum value of 0.69 rad (Fig. 3g). In contrast, the precision limit associated with the maximum information state equals 0.067 rad, an entire order of magnitude smaller than the minimum value measured for plane waves. While reaching this precision limit would require amplitude and phase modulation of the incident field, we only modulate its phase by the input SLM in the experiment. We find that the precision limit associated with phase-only modulation of the maximum information state equals 0.077 rad, a value that is only slightly larger than that for a joint amplitude and phase modulation. This observation corroborates that our approach is also very robust with respect to small errors or imperfections in the prepa-

ration of the incident state.

In order to demonstrate the practical implementation of the estimation process with a maximum information state, we inject it in the medium and perform a sequence of measurements. The observable parameter we estimate is the phase shift φ induced by the cross-shaped target, which is varied every 20 measurements between -0.25 rad and 0.25 rad in a step-like manner (Fig. 4a). From the knowledge of the expected outgoing state and its derivative with respect to φ , we can construct the minimum variance unbiased estimator of φ , applicable to small parameter variations (see Supplementary Information S2.3). We can then estimate the value of φ from measurements of the outgoing state (see Extended Data Fig. 1). Even though only approximately 24,000 incident photons are probing the medium per measurement, each step can be clearly resolved (Fig. 4b,c). We observe

a bias of -0.18 rad, which can appear due to small errors in the measured reflection matrix. After subtracting this bias, the observed standard error on the estimates is 0.10 rad, which corresponds to a transverse displacement of the target of 8.7 nm. Importantly, the observed standard error on the estimates almost reaches the precision limit predicted by the Cramér-Rao inequality. This confirms that shot noise is the dominant source of noise in our experiment, and demonstrates that the precision limit is correctly predicted from reflection matrix measurements. We applied the same procedure for measurements performed by injecting the best plane wave used to construct the reflection matrix. The precision limit (0.69 rad) is then much larger than the step size, thereby prohibiting the detection of the phase steps (Fig. 4d,e).

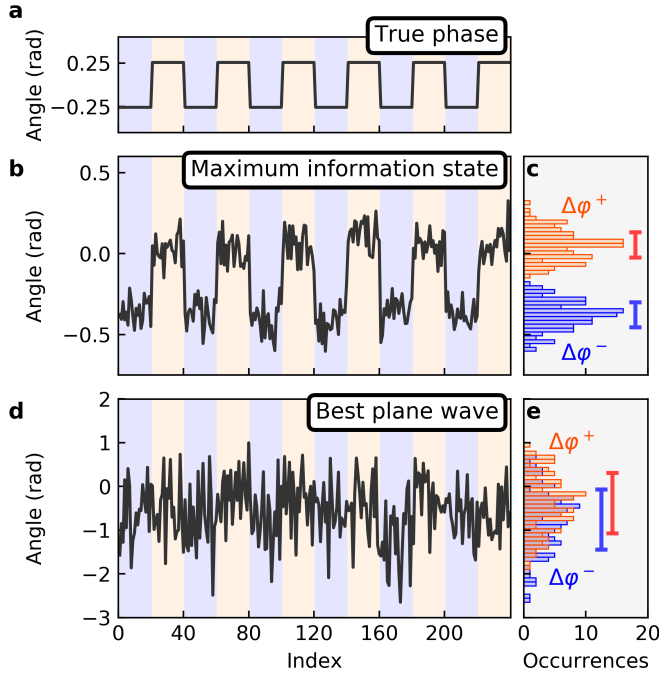


Fig. 4 | Demonstration of optimal estimations. **a**, Step-like function applied to the five cross-shaped pixels on the hidden SLM to modulate the phase shift induced by the target during the acquisition. **b**, Estimated phase shift as a function of measurement index for measurements performed by injecting the maximum information state. **c**, Histograms of estimated angles for a positive phase shift ($\Delta\varphi^+ = +0.25$ rad) and a negative phase shift ($\Delta\varphi^- = -0.25$ rad) applied by the hidden SLM. The length of error bars equals $2\sigma_{\text{CRB}}$. **d**, **e**, Analogous to **b** and **c** for measurements performed by injecting the best plane wave.

To summarize, we introduce a general framework to perform optimal measurements in wave scattering environments. We establish a fundamental limit to the precision of coherent scattering measurements for any observable of interest and demonstrate that this limit can be reached in an experiment. As a feedback mechanism to identify optimal light states, we modulate the phase

of a target displayed by an SLM. We envision that many different mechanisms could be used in future work, for instance using ultrasound-based techniques [23–25], photothermal contrast [26] or taking advantage of the spontaneous motion of a target [27, 28]. We emphasize that our results are generally applicable to any parametric dependence of a wave field and can thus be easily transposed to other types of waves such as in acoustics [29] or in the microwave regime [30]. Finally, it can be expected that the classical bound derived in this work will be surpassed using quantum metrology protocols [11, 31, 32]. In this context, our results provide a general benchmark to assess the performance of quantum states optimized for parameter estimation, and suggest a new path towards the identification of optimally-sensitive quantum states of light using scattering matrices of complex systems.

Acknowledgements. The authors thank M. van Beurden, J. Bosch, S. Faez, M. Horodynski, M. Kühmayer, P. Pai, and J. Seifert for insightful discussions, and P. Jurrius, D. Killian and C. de Kok for technical support. This work was supported by the Netherlands Organization for Scientific Research (Vici 68047618 and Perspective P16-08) and by the Austrian Science Fund (FWF) under project number P32300 (WAVELAND).

[1] Y. Park, C. Depeursinge, and G. Popescu, *Nat. Photonics* **12**, 578 (2018).

[2] R. W. Taylor and V. Sandoghdar, *Nano Lett.* **19**, 4827 (2019).

[3] W. Osten and N. Reingand, *Optical Imaging and Metrology: Advanced Technologies* (John Wiley & Sons, 2012).

[4] E. G. van Putten, A. Lagendijk, and A. P. Mosk, *Opt. Lett.* **37**, 1070 (2012).

[5] Y. Shechtman, S. J. Sahl, A. S. Backer, and W. E. Moerner, *Phys. Rev. Lett.* **113**, 133902 (2014).

[6] F. Balzarotti, Y. Eilers, K. C. Gwosch, A. H. Gynnå, V. Westphal, F. D. Stefani, J. Elf, and S. W. Hell, *Science* **355**, 606 (2017).

[7] P. Ambichl, W. Xiong, Y. Bromberg, B. Redding, H. Cao, and S. Rotter, *Phys. Rev. X* **7**, 041053 (2017).

[8] G. H. Yuan and N. I. Zheludev, *Science* **364**, 771 (2019).

[9] D. Bouchet, R. Carminati, and A. P. Mosk, *arXiv:1909.02501* (2019).

[10] T. Juffmann, A. de los Ríos Sommer, and S. Gigan, *Opt. Commun.* **454**, 124484 (2020).

[11] V. Giovannetti, S. Lloyd, and L. Maccone, *Nat. Photonics* **5**, 222 (2011).

[12] S. M. Popoff, G. Lerosey, R. Carminati, M. Fink, A. C. Boccara, and S. Gigan, *Phys. Rev. Lett.* **104**, 100601 (2010).

[13] S. Rotter and S. Gigan, *Rev. Mod. Phys.* **89**, 015005 (2017).

[14] H. H. Barrett and K. J. Myers, *Foundations of Image Science* (John Wiley & Sons, 2013).

[15] S. Kay, *Fundamentals of Statistical Processing, Volume I: Estimation Theory* (Prentice Hall, 1993).

- [16] P. Ambichl, A. Brandstötter, J. Böhm, M. Kühmayer, U. Kuhl, and S. Rotter, *Phys. Rev. Lett.* **119**, 033903 (2017).
- [17] M. Horodynski, M. Kühmayer, A. Brandstötter, K. Pichler, Y. V. Fyodorov, U. Kuhl, and S. Rotter, *Nat. Photonics* (2019).
- [18] A. P. Mosk, A. Lagendijk, G. Leroosey, and M. Fink, *Nat. Photonics* **6**, 283 (2012).
- [19] S. L. Braunstein, C. M. Caves, and G. J. Milburn, *Ann. Phys. (N. Y.)* **247**, 135 (1996).
- [20] H. Yu, T. R. Hillman, W. Choi, J. O. Lee, M. S. Feld, R. R. Dasari, and Y. Park, *Phys. Rev. Lett.* **111**, 153902 (2013).
- [21] J. Carpenter, B. J. Eggleton, and J. Schröder, *Nat. Photonics* **9**, 751 (2015).
- [22] W. Xiong, P. Ambichl, Y. Bromberg, B. Redding, S. Rotter, and H. Cao, *Phys. Rev. Lett.* **117**, 053901 (2016).
- [23] X. Xu, H. Liu, and L. V. Wang, *Nat. Photonics* **5**, 154 (2011).
- [24] B. Judkewitz, Y. M. Wang, R. Horstmeyer, A. Mathy, and C. Yang, *Nat. Photonics* **7**, 300 (2013).
- [25] O. Katz, F. Ramaz, S. Gigan, and M. Fink, *Nat. Commun.* **10**, 717 (2019).
- [26] A. Gaiduk, M. Yorulmaz, P. V. Ruijgrok, and M. Orrit, *Science* **330**, 353 (2010).
- [27] E. H. Zhou, H. Ruan, C. Yang, and B. Judkewitz, *Optica* **1**, 227 (2014).
- [28] C. Ma, X. Xu, Y. Liu, and L. V. Wang, *Nat. Photonics* **8**, 931 (2014).
- [29] B. Gérardin, J. Laurent, A. Derode, C. Prada, and A. Aubry, *Phys. Rev. Lett.* **113**, 173901 (2014).
- [30] Z. Shi and A. Z. Genack, *Phys. Rev. Lett.* **108**, 043901 (2012).
- [31] V. Giovannetti, S. Lloyd, and L. Maccone, *Phys. Rev. Lett.* **96**, 010401 (2006).
- [32] L. J. Fiderer, J. M. E. Fraïsse, and D. Braun, *Phys. Rev. Lett.* **123**, 250502 (2019).
- [33] P. Pai, J. Bosch, and A. P. Mosk, [arXiv:1912.00933](https://arxiv.org/abs/1912.00933) (2019).
- [34] M. Takeda, H. Ina, and S. Kobayashi, *J. Opt. Soc. Am.* **72**, 156 (1982).
- [35] E. Cuche, P. Marquet, and C. Depeursinge, *Appl. Opt.* **39**, 4070 (2000).

METHODS

Optical setup. The light source is a continuous wave solid-state laser (Coherent OBIS 532-120 LS FP) emitting at 532 nm. The laser light is coupled to a single-mode polarization-maintaining fiber and out-coupled using a collimator (Schäfter-Kirchhoff, 60FC-L-4-M75-01). The beam is separated into a signal path and a reference path using a 50:50 beamsplitter. In the signal path, the light beam passes a 50:50 beamsplitter and is then modulated by the input SLM (Holoeye Pluto VIS). It can then pass different neutral density filters which are mechanically placed or removed. The incident power on the objective is: 36.1 μW when all density filters are removed from the optical path; 275 nW when a neutral density filter

of optical density 2 (ND2) is placed in the optical path (measured fractional transmittance $\mathcal{T}' = 0.76 \times 10^{-2}$); 30 pW when a neutral density filter of optical density 6 (ND6) is placed in the optical path (measured fractional transmittance $\mathcal{T} = 0.83 \times 10^{-6}$).

The surface of the SLM is imaged onto a ground glass diffuser using a 4f system composed by a 200 mm lens and a $\times 50$ objective (Nikon 50X CFI60 TU Plan Epi ELWD, 0.6 NA). A 90:10 beamsplitter is located between the lens and the objective. The diffuser is made by polishing a microscope coverslip. The resulting scattering angle, defined from the full width at half maximum of the transmitted intensity distribution, is approximately 15° . The diffuser is mounted on the windows of the hidden SLM (Holoeye Pluto BB) at a distance of 1.2 mm. The surface of the diffuser is then imaged using a 4f system composed by the objective and a 200 mm lens using a CCD camera (AVT Stingray F145-B) with an exposure time of 300 μs . Before reaching the camera, the beam passes a polarizer to ensure that only the horizontal component of the field is measured, and also passes a 90:10 beamsplitter to recombine the reference path with the signal path. Camera acquisition is triggered by the input SLM in order to limit phase noise due to the flicker of the SLM.

Construction of the reflection matrix and its derivative. We construct densely-sampled reflection matrices relating incident field states to reflected ones [33]. Reflection matrix measurements are performed with no density filter in the signal path. To illuminate the medium, we vary the incidence angle of a Gaussian beam characterized by a full-width at half maximum of 120 μm , which is 4 times larger than the field of view (such Gaussian beams are referred to as plane waves in the manuscript). We probe $M = 2437$ different incidence angles, covering a numerical aperture of 0.5. The sampling is performed using a triangular lattice (in Fourier space), with a lattice constant taken to be the smallest angular separation at which the complex inner product of nearest-neighbor fields drops to zero.

For each incident angle, we record the reflected field using digital off-axis holography [34, 35]. The method relies on a reference beam which is tilted by an angle with respect to the reflected signal beam. The complex field is then numerically reconstructed from the measured holograms by digitally filtering the zero-order component. The reflected field is sampled using a triangular lattice, with a lattice constant that we determine by finding the distance between the maximum and the first minimum of the autocorrelation of a random field. We use $N = 2465$ different sampling points, covering an area of 890 μm^2 on the surface of the diffuser.

The reflection matrix r is therefore constructed column by column. As a result, we obtain a 2465×2437 matrix. This reflection matrix is measured at an angle $\varphi = \varphi_0$ for the phase shift induced by the hidden target,

which can be arbitrarily set to zero. In order to estimate the derivative of the reflection matrix with respect to φ , we measure two other reflection matrices $r(\varphi_0 - \Delta\varphi)$ and $r(\varphi_0 + \Delta\varphi)$, where $\Delta\varphi = 0.54$ rad. We can then estimate $\partial_\varphi r$ by applying the centered finite difference scheme $\partial_\varphi r \simeq [r(\varphi_0 + \Delta\varphi) - r(\varphi_0 - \Delta\varphi)]/(2\Delta\varphi)$.

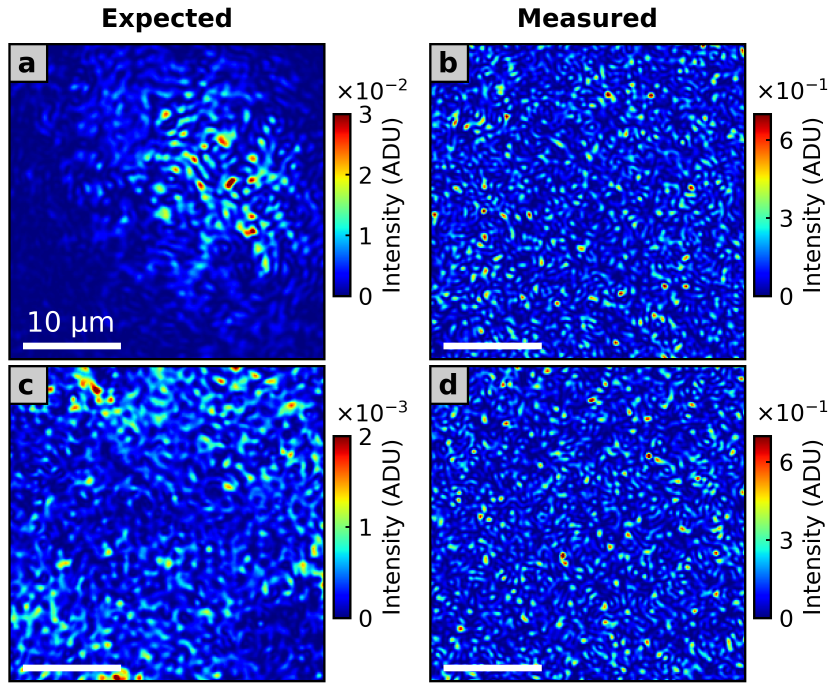
Monitoring of the global phase drift. Due to the significant acquisition time (76 min in total), the global phase of the measured outgoing field slowly drifts in time because of the imperfect thermal stability of the experimental setup. During the acquisition, we continuously monitor this drift by regularly measuring a known outgoing field as a phase reference [33]. We use different phase-reference fields depending on the incident power on the sample.

When no density filters are placed in the optical path, the phase-reference field is generated by injecting a given plane wave in the medium, with a slight angle so that no reflection from the back-focal plane of the objective can be observed. We then calculate how the global phase of this field changes over time by using a complex inner

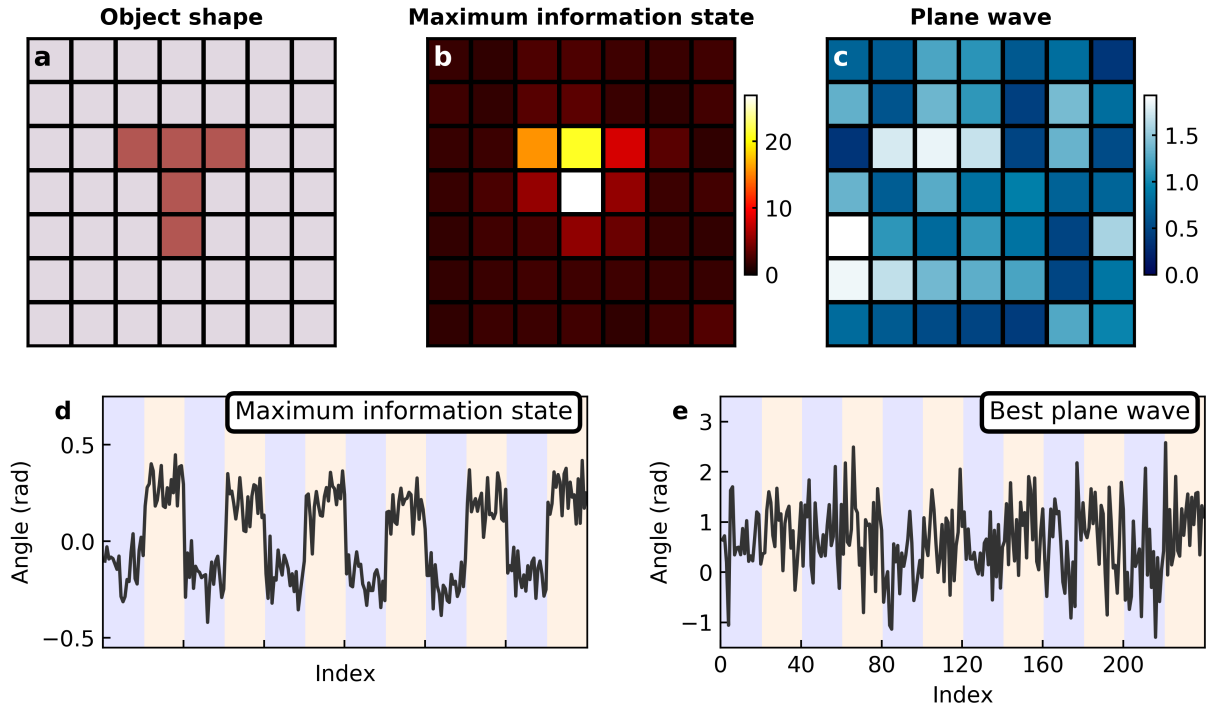
product of the phase-reference field measured at a given time with the phase-reference field measured at the beginning of the acquisition.

When any density filter is placed in the optical path (ND2 or ND6), we first calculate a truncated reflection matrix r' , which does not include the few columns for which reflection from the back-focal plane of the objective can be observed. The phase-reference field is generated by injecting the right-singular vector of r' associated with its largest singular value. By doing so, we maximize the signal-to-noise ratio of phase-reference measurements. We then calculate how the global phase of this field changes over time by using a complex inner product of the phase-reference field measured at a given time with the field predicted from the knowledge of the reflection matrix.

Finally, we perform linear interpolations for estimating the global phase drift at any time during the acquisition, and we subsequently apply the appropriate phase correction to any measured data.



Extended Data Fig. 1. | Expected and measured signal intensity distribution at low photon counts. **a, b**, Expected signal intensity for the optimal incident state and for the best plane wave expressed in analog-to-digital units (ADU) and calculated when ND6 is in the signal path. **c, d**, Measured signal intensity for the optimal incident state and for the best plane wave, corresponding to the first point of phase step measurements. Due to the presence of ND6 in the signal path, the signal-to-noise per pixel is largely smaller than unity for the measurements. However, when applying the minimum variance unbiased estimator, data measured by illuminating the medium with the optimal incident state allow to correctly estimate the phase for the hidden target. This can be achieved since only one parameter (the phase shift induced by the target) must be estimated from a large number of independent sampling points.



Extended Data Fig. 2. | Maximum information state for a different object shape. **a**, Geometry of a different hidden object displayed by the hidden SLM, in the shape of the letter "T". The edge size of a pixel is $16\text{ }\mu\text{m}$ (we define a pixel as an ensemble of four physical pixels of the hidden SLM). **b**, Fisher information associated with each pixel in the target area for the optimal state, normalized by the average Fisher information under plane-wave illumination. The optimal state defined with respect to this new target is primarily sensitive to the 5 pixels defining the letter "T". However, the intensity does not need to be uniformly distributed on this area, which explains why the shape of the target is not fully revealed here. **c**, Analogous to **b** for plane-wave illumination, which shows that the sensitivity of a plane wave randomly varies with the considered pixel. **d**, Estimated phase shift as a function of measurement index for measurements performed by injecting the optimal incident state, when ND6 is in the signal path. The phase shift induced by the hidden object is varied every 20 measurements between -0.25 rad and 0.25 rad in a step-like manner. The precision limit calculated for these measurements is 0.083 rad . **e**, Analogous to **d** for measurements performed by injecting the best plane wave. The precision limit calculated for these measurements is 0.65 rad .

Maximum information states for coherent scattering measurements

Supplementary information

Dorian Bouchet,¹ Stefan Rotter,² and Allard P. Mosk¹

¹ *Nanophotonics, Debye Institute for Nanomaterials Science,*

Utrecht University, P.O. Box 80000, 3508 TA Utrecht, the Netherlands

² *Institute for Theoretical Physics, Vienna University of Technology (TU Wien), A-1040 Vienna, Austria*

SUPPLEMENTARY SECTION S1 – FISHER INFORMATION FOR THE OPTIMAL DETECTION SCHEME

In this section, we calculate the classical Fisher information for the optimal homodyne detection scheme, which we show to be equal to the quantum Fisher information for coherent states and statistically independent samples. We then define the Fisher information operator from the scattering matrix of the system, and we provide the expression of the minimum variance unbiased estimator.

S1.1 – Classical Fisher information

Let us describe the measured data by a N -dimensional random variable X and a joint probability density function $p(X; \theta)$ parameterized by an arbitrary parameter θ . In general, the Fisher information is expressed by [1]

$$\mathcal{J}(\theta) = \mathbb{E} ([\partial_\theta \ln p(X; \theta)]^2) , \quad (\text{S1})$$

where \mathbb{E} denotes the expectation operator acting over noise fluctuations. In the case of scattering measurements performed with a homodyne detection scheme with a strong reference beam, readout noise can be neglected. The signal measured at the k -th sampling point can then be modeled by a Poisson distribution of expectation $I_k^{\text{tot}} = |E_k^{\text{out}} + E_k^{\text{ref}}|^2$, where E_k^{out} and E_k^{ref} are the complex values of the outgoing signal field and of the reference field, respectively. Considering N statistically independent sampling points, the joint probability density function $p(X; \theta)$ is therefore expressed by

$$p(X; \theta) = \prod_{k=1}^N e^{-|E_k^{\text{out}} + E_k^{\text{ref}}|^2} \frac{|E_k^{\text{out}} + E_k^{\text{ref}}|^{2X_k}}{X_k!} . \quad (\text{S2})$$

Injecting this expression in Eq. (S1), we obtain

$$\mathcal{J}(\theta) = \sum_{k=1}^N \frac{[\partial_\theta (|E_k^{\text{out}} + E_k^{\text{ref}}|^2)]^2}{|E_k^{\text{out}} + E_k^{\text{ref}}|^2} . \quad (\text{S3})$$

For a strong reference field which does not depend on θ (i.e., for $|E_k^{\text{ref}}|^2 \gg |E_k^{\text{out}}|^2$ and $\partial_\theta E_k^{\text{ref}} = 0$), this expression simplifies to

$$\mathcal{J}(\theta) = \sum_{k=1}^N \frac{\left(\partial_\theta \left[E_k^{\text{out}} (E_k^{\text{ref}})^* + E_k^{\text{ref}} (E_k^{\text{out}})^* \right] \right)^2}{|E_k^{\text{ref}}|^2} . \quad (\text{S4})$$

We now introduce $E_k^{\text{out}} = Q_k^{\text{out}} + i P_k^{\text{out}}$ and $E_k^{\text{ref}} = |E_k^{\text{ref}}| e^{i\phi_k}$. Equation (S4) becomes

$$\mathcal{J}(\theta) = 4 \sum_{k=1}^N \left[(\partial_\theta Q_k^{\text{out}}) \cos \phi_k + (\partial_\theta P_k^{\text{out}}) \sin \phi_k \right]^2 . \quad (\text{S5})$$

For any integer m , the phase angles of the reference field which maximize Eq. (S5) are given by $\phi_k^{\max} = \arg(\partial_\theta E_k^{\text{out}}) + m\pi$, and those which minimize Eq. (S5) are given by $\phi_k^{\min} = \arg(\partial_\theta E_k^{\text{out}}) + (m+1/2)\pi$. Choosing ϕ_k^{\min} as phase angles of the reference field yields $\mathcal{J}(\theta) = 0$. In contrast, choosing ϕ_k^{\max} as phase angles of the reference field yields

$$\mathcal{J}(\theta) = 4 \sum_{k=1}^N |\partial_\theta E_k^{\text{out}}|^2. \quad (\text{S6})$$

This expression can be identified as the Fisher information for a random vector composed of N complex random variables whose real and imaginary parts are independent normally distributed random variables with variance $\sigma^2 = 1/4$.

S1.2 – Quantum Fisher information

The classical Fisher information $\mathcal{J}(\theta)$ sets a lower bound on the variance of unbiased estimators of θ for a definite measurement scheme (i.e. the homodyne scheme in our case). A more general lower bound exists, which applies to any quantum measurement described by a positive-operator-valued measure (POVM). This lower bound is given by the reciprocal of the quantum Fisher information, which is expressed by [2]

$$\mathcal{I}(\theta) = \text{Tr}(\rho_{\text{out}} L_{\text{out}}^2), \quad (\text{S7})$$

where ρ_{out} is a density operator describing the quantum state of the system and L_{out} is the symmetrized logarithmic derivative of ρ_{out} with respect to θ defined as follows:

$$\rho_{\text{out}} L_{\text{out}} + L_{\text{out}} \rho_{\text{out}} = 2 \partial_\theta \rho_{\text{out}}. \quad (\text{S8})$$

Considering that ρ_{out} describes a N -modes coherent state composed of simply-separable pure states, Eq. (S7) simplifies to [3, 4]

$$\mathcal{I}(\theta) = 4 \sum_{k=1}^N (\langle \partial_\theta \alpha_k | \partial_\theta \alpha_k \rangle - |\langle \partial_\theta \alpha_k | \alpha_k \rangle|^2), \quad (\text{S9})$$

where $|\alpha_k\rangle$ is the single-mode coherent state associated with the k -th mode and $|\partial_\theta \alpha_k\rangle$ is its derivative with respect to θ . We can represent $|\alpha_k\rangle$ in the basis of Fock states $|n\rangle$ labeled by the occupation number n , which reads [5]

$$|\alpha_k\rangle = e^{-|\alpha_k|^2/2} \sum_{n=0}^{\infty} \frac{\alpha_k^n}{(n!)^{1/2}} |n\rangle, \quad (\text{S10})$$

where α_k denotes the eigenvalue of the annihilation operator. Taking the derivative of this expression with respect to θ leads to

$$|\partial_\theta \alpha_k\rangle = \partial_\theta \alpha_k \left[-|\alpha_k| e^{-|\alpha_k|^2/2} \sum_{n=0}^{\infty} \frac{\alpha_k^n}{(n!)^{1/2}} |n\rangle + e^{-|\alpha_k|^2/2} \sum_{n=1}^{\infty} \frac{n \alpha_k^{n-1}}{(n!)^{1/2}} |n\rangle \right]. \quad (\text{S11})$$

We can now use Eqs. (S10) and (S11) to calculate the two terms $\langle \partial_\theta \alpha_k | \partial_\theta \alpha_k \rangle$ and $|\langle \partial_\theta \alpha_k | \alpha_k \rangle|^2$ that appear in Eq. (S9). Let us first calculate $\langle \partial_\theta \alpha_k | \partial_\theta \alpha_k \rangle$ from Eq. (S11): using the orthonormality of Fock states, we obtain

$$\begin{aligned} \langle \partial_\theta \alpha_k | \partial_\theta \alpha_k \rangle = & |\partial_\theta \alpha_k|^2 \left[|\alpha_k|^2 e^{-|\alpha_k|^2} \sum_{n=0}^{\infty} \frac{|\alpha_k|^{2n}}{n!} - |\alpha_k| \alpha_k e^{-|\alpha_k|^2} \sum_{n=1}^{\infty} \frac{|\alpha_k|^{2(n-1)}}{(n-1)!} \right. \\ & \left. - |\alpha_k| \alpha_k^* e^{-|\alpha_k|^2} \sum_{n=1}^{\infty} \frac{|\alpha_k|^{2(n-1)}}{(n-1)!} + e^{-|\alpha_k|^2} \sum_{n=1}^{\infty} \frac{n |\alpha_k|^{2(n-1)}}{(n-1)!} \right]. \end{aligned} \quad (\text{S12})$$

This expression can be simplified by using the following properties of exponential series:

$$\sum_{n=0}^{\infty} \frac{|\alpha_k|^{2n}}{n!} = e^{|\alpha_k|^2}, \quad (\text{S13})$$

$$\sum_{n=0}^{\infty} \frac{(n+1)|\alpha_k|^{2n}}{n!} = (1 + |\alpha_k|^2)e^{|\alpha_k|^2}. \quad (\text{S14})$$

Injecting Eqs. (S13) and (S14) into Eq. (S12) leads to

$$\langle \partial_{\theta} \alpha_k | \partial_{\theta} \alpha_k \rangle = |\partial_{\theta} \alpha_k|^2 (2|\alpha_k|^2 - |\alpha_k| \alpha_k - |\alpha_k| \alpha_k^* + 1). \quad (\text{S15})$$

Let us now calculate $\langle \partial_{\theta} \alpha_k | \alpha_k \rangle$ from Eqs. (S10) and (S11): using again the orthonormality of Fock states, we obtain

$$\langle \partial_{\theta} \alpha_k | \alpha_k \rangle = \partial_{\theta} \alpha_k^* \left[-|\alpha_k| e^{-|\alpha_k|^2} \sum_{n=0}^{\infty} \frac{|\alpha_k|^{2n}}{n!} + \alpha_k e^{-|\alpha_k|^2} \sum_{n=1}^{\infty} \frac{|\alpha_k|^{2(n-1)}}{(n-1)!} \right]. \quad (\text{S16})$$

Injecting Eq. (S13) into Eq. (S16) leads to

$$|\langle \partial_{\theta} \alpha_k | \alpha_k \rangle|^2 = |\partial_{\theta} \alpha_k|^2 (2|\alpha_k|^2 - |\alpha_k| \alpha_k - |\alpha_k| \alpha_k^*). \quad (\text{S17})$$

Finally, injecting Eqs. (S15) and (S17) into Eq. (S9) results in

$$\mathcal{I}(\theta) = 4 \sum_{k=1}^N |\partial_{\theta} \alpha_k|^2. \quad (\text{S18})$$

We can use the same quantum-mechanical formalism to derive the classical Fisher information for the homodyne detection scheme. To this end, we consider the coherent state $|\alpha_k, r_k\rangle = |\alpha_k + r_k\rangle$ which represents the superposition of the coherent state $|\alpha_k\rangle$ with a reference coherence state $|r_k\rangle$. The probability to observe n_k photons in the state $|\alpha_k, r_k\rangle$ is $\mathcal{P}_k = |\langle n_k | \alpha_k + r_k \rangle|^2$, which leads to a Poisson distribution of expectation value $|\alpha_k + r_k|^2$. In the same way that we obtained Eq. (S6) from Eq. (S1) with classical fields, we now obtain

$$\mathcal{J}(\theta) = 4 \sum_{k=1}^N |\partial_{\theta} \alpha_k|^2. \quad (\text{S19})$$

The classical Fisher information given by Eq. (S19) equals the quantum Fisher information given by Eq. (S18), thereby ensuring that the homodyne detection scheme that we considered is optimal for the estimation of θ .

S1.3 – Fisher information operator

In the formalism of the S -matrix, the outgoing field state is expressed by $E^{\text{out}} = SE^{\text{in}}$, where S denotes the scattering matrix (or S -matrix) and E^{in} is the incident field state. We can write E_k^{out} as a projection of the outgoing state on the state associated with the k -th sampling point, which we write as $E_k^{\text{out}} = \langle k | S | E^{\text{in}} \rangle$ in bra-ket notations, leading to

$$\mathcal{J}(\theta) = 4 \sum_{k=1}^N |\langle k | \partial_{\theta} S | E^{\text{in}} \rangle|^2. \quad (\text{S20})$$

This expression can be expanded into

$$\mathcal{J}(\theta) = 4 \sum_{k=1}^N \langle E^{\text{in}} | (\partial_{\theta} S)^{\dagger} | k \rangle \langle k | \partial_{\theta} S | E^{\text{in}} \rangle. \quad (\text{S21})$$

Using the completeness relation $\sum_k |k\rangle \langle k| = I_N$ where I_N is the N -dimensional identity matrix, we finally obtain

$$\mathcal{J}(\theta) = 4 \langle E^{\text{in}} | (\partial_{\theta} S)^{\dagger} \partial_{\theta} S | E^{\text{in}} \rangle. \quad (\text{S22})$$

In this expression, we can identify the operator $F_{\theta} = 4(\partial_{\theta} S)^{\dagger} \partial_{\theta} S$, which we refer to as *Fisher information operator*. We obtain the quadratic form $\mathcal{J}(\theta) = \langle E^{\text{in}} | F_{\theta} | E^{\text{in}} \rangle$, which is the expression of the Fisher information given in the manuscript. Finally, for a unitary scattering matrix ($S^{\dagger} = S^{-1}$), the operator F_{θ} is expressed by

$$F_{\theta} = (-2iS^{-1}\partial_{\theta} S)^2, \quad (\text{S23})$$

where we used the identity $\partial_\theta S^{-1} = -S^{-1}(\partial_\theta S)S^{-1}$. Introducing the generalized Wigner-Smith operator [6], which is defined by $Q_\theta = -iS^{-1}\partial_\theta S$, we obtain the identity

$$F_\theta = 4Q_\theta^2, \quad (\text{S24})$$

which implies that F_θ and Q_θ share the same eigenstates. Writing the eigenvalue equation $Q_\theta E^{\text{in}} = \Lambda E^{\text{in}}$ where we choose Λ as the eigenvalue of Q_θ with the largest absolute value, we obtain $\partial_\theta E^{\text{out}} = i\Lambda E^{\text{out}}$. For a scattering matrix evaluated at θ_0 and a small parameter variation $\Delta\theta = \theta - \theta_0$, this results in $E^{\text{out}}(\theta) \simeq e^{i\Lambda\Delta\theta} E^{\text{out}}(\theta_0)$. Thus, in the limit of a unitary scattering matrix, maximum information states are insensitive with respect to small variations in θ except for a global phase factor.

S1.4 – Minimum variance unbiased estimator

For small parameter variations around a given parameter value noted θ_0 , the measured data X can be described by the following linear model:

$$X = I^{\text{tot}} + (\partial_\theta I^{\text{tot}})(\theta - \theta_0) + W, \quad (\text{S25})$$

where I^{tot} and $\partial_\theta I^{\text{tot}}$ are evaluated at θ_0 , and where W is a random vector composed of N independent and normally distributed random variables with mean zero and variance I_k^{tot} . The normal distribution is indeed a good approximation of the Poisson distribution for large expectation values. In the case of linear models, general expressions exist for the minimum variance unbiased estimator, which depends on the noise statistics [1]. For the linear model expressed by Eq. (S25), the minimum variance unbiased estimator reads

$$\hat{\theta}(X) - \theta_0 = \frac{1}{\mathcal{J}(\theta_0)} \sum_{k=1}^N \frac{(\partial_\theta I_k^{\text{tot}})(X_k - I_k^{\text{tot}})}{I_k^{\text{tot}}}. \quad (\text{S26})$$

Writing $I_k^{\text{tot}} = |E_k^{\text{out}} + E_k^{\text{ref}}|^2$ and recalling that $|E_k^{\text{ref}}|^2 \gg |E_k^{\text{out}}|^2$ and $\partial_\theta E_k^{\text{ref}} = 0$, this expression simplifies to

$$\hat{\theta}(X) - \theta_0 = \frac{1}{\mathcal{J}(\theta_0)} \sum_{k=1}^N \frac{\left(\partial_\theta \left[E_k^{\text{out}} (E_k^{\text{ref}})^* + E_k^{\text{ref}} (E_k^{\text{out}})^* \right]\right) (X_k - |E_k^{\text{out}} + E_k^{\text{ref}}|^2)}{|E_k^{\text{ref}}|^2}. \quad (\text{S27})$$

Introducing $E_k^{\text{ref}} = |E_k^{\text{ref}}|e^{i\phi_k}$ and using the phase angles $\phi_k^{\text{max}} = \arg(\partial_\theta E_k^{\text{out}})$ which maximize the Fisher information leads to

$$\hat{\theta}(X) - \theta_0 = \frac{2}{\mathcal{J}(\theta_0)} \sum_{k=1}^N \frac{|\partial_\theta E_k^{\text{out}}|(X_k - |E_k^{\text{out}} + E_k^{\text{ref}}|^2)}{|E_k^{\text{ref}}|}. \quad (\text{S28})$$

In this expression, $\mathcal{J}(\theta_0)$ is obtained from Eq. (S6), E_k^{out} is obtained from $E_k^{\text{out}} = \langle k | S | E^{\text{in}} \rangle$ and $\partial_\theta E_k^{\text{out}}$ is obtained from $\partial_\theta E_k^{\text{out}} = \langle k | \partial_\theta S | E^{\text{in}} \rangle$, with a scattering matrix S evaluated at θ_0 .

SUPPLEMENTARY SECTION S2 – FISHER INFORMATION IN THE EXPERIMENT

In this section, we give the expression of the Fisher information for our experiment, we verify the noise statistics of the quadrature components of the field, and we provide the expression of the minimum variance unbiased estimator used in the experiment.

S2.1 – Expression of the Fisher information in the experiment

In our proof-of-principle experiment, the reference beam is not optimally shaped but consists of a tilted plane wave. In this case, the Fisher information is obtained by averaging Eq. (S5) over the phase angle of the reference beam:

$$\mathcal{J}(\varphi) = 4 \sum_{k=1}^N \int_0^{2\pi} d\phi \left[(\partial_\varphi Q_k^{\text{out}}) \cos \phi + (\partial_\varphi P_k^{\text{out}}) \sin \phi \right]^2. \quad (\text{S29})$$

We obtain the following simplified expression:

$$\mathcal{J}(\varphi) = 2 \sum_{k=1}^N |\partial_\varphi E_k^{\text{out}}|^2. \quad (\text{S30})$$

Note that this expression is identical to the expression of the optimal Fisher information given in Eq. (S6), except for a factor of two. Hence, the incoming state which maximizes Eq. (S30) also maximizes Eq. (S6).

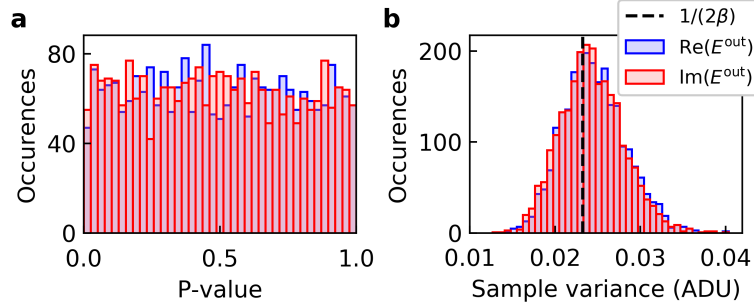
In the experiment, we must also take into account two additional considerations. First, the value of the $N = 2465$ sampling points are actually estimated from $N_{\text{cam}} = 53044$ statistically independent camera pixels (oversampling is required in off-axis holography). The oversampling ratio $\beta = N_{\text{cam}}/N$ must therefore be included as a prefactor in Eq. (S30). Moreover, while we measured the reflection matrix without any neutral density filter, we consistently use the strongest neutral density filter ND6 (fractional transmittance $\mathcal{T} = 0.83 \times 10^{-6}$) to compute all values of the Fisher information. Therefore, the expression of the Fisher information relevant to our experiment is

$$\mathcal{J}(\varphi) = \frac{\mathcal{T}}{\sigma^2} \langle E^{\text{in}} | (\partial_\varphi r)^\dagger \partial_\varphi r | E^{\text{in}} \rangle, \quad (\text{S31})$$

where we noted $\sigma^2 = 1/(2\beta)$ in order to highlight that this expression can be identified as the Fisher information for a random vector composed of N complex random variables whose real and imaginary parts are independent normally distributed random variables with variance σ^2 . The precision limit σ_{CRB} , which bounds the standard deviation of any estimator of φ in our experiment, is then expressed from Eq. (S31) by $\sigma_{\text{CRB}} = \mathcal{J}^{-1/2}$.

S2.2 – Gaussian distribution of the quadrature components of the field

We can verify that the measured quadrature components of the field follow a Gaussian distribution when the neutral density filter ND6 is in the signal path. To this end, we inject the optimal incident state in the medium and perform 100 successive measurements of the outgoing field. We then compute the p-value for each sampling point according to the Shapiro-Wilk test. The uniform distribution of p-value (Fig. S1a) confirms that the measured quadrature components of the field follow a Gaussian distribution. We also construct the histogram of the sample variance (Fig. S1b), with a mean value of 0.0244 ADU. This value is in good agreement with the theoretical value given by $1/(2\beta) = 0.0232$ ADU. We consistently choose the mean value experimentally determined ($\sigma^2 = 0.0244$ ADU) to calculate the Fisher information in Eq. (S31).



Supplementary Figure S1 | Statistics of the quadrature components of the field. **a**, P-value distribution for the 2465 sampling points. The p-value for each point is calculated using Shapiro-Wilk test statistics from 100 different realization of the random noise. **b**, Distribution of the sample variance for the 2465 sampling points.

S2.3 – Phase-step estimations

For small variations of φ around φ_0 , measured data can be described by the following linear model:

$$X = E^{\text{out}} + (\partial_\varphi E^{\text{out}})(\varphi - \varphi_0) + W, \quad (\text{S32})$$

where X represents here the complex field retrieved from the measured data using off-axis holography, where E^{out} and $\partial_\varphi E^{\text{out}}$ are evaluated at φ_0 , and where W is a complex random vector composed of N complex random variables whose real and imaginary parts are independent normally distributed random variables with mean zero and variance σ^2 . For this linear model, the minimum variance unbiased estimator reads [1]

$$\hat{\varphi}(X) - \varphi_0 = \frac{\text{Re} [\langle \partial_\varphi E^{\text{out}} | X \rangle - \langle \partial_\varphi E^{\text{out}} | E^{\text{out}} \rangle]}{\langle \partial_\varphi E^{\text{out}} | \partial_\varphi E^{\text{out}} \rangle}. \quad (\text{S33})$$

During phase-steps measurements, the neutral density filter ND6 (characterized by a fractional transmittance \mathcal{T}) is placed in the signal optical path. Moreover, due to measurement noise during reflection matrix measurements, the intensity and the Fisher information predicted from the knowledge of the reflection matrix differ from direct measurements by a factor η_i and η_F , respectively (see Supplementary Information S3). The estimator of φ associated with our experimental setup is thus obtained from Eq. (S33) by taking $|E^{\text{out}}\rangle = (\eta_i \mathcal{T})^{1/2} r |\tilde{E}^{\text{in}}\rangle$ and $|\partial_\varphi E^{\text{out}}\rangle = (\eta_F \mathcal{T})^{1/2} \partial_\varphi r |\tilde{E}^{\text{in}}\rangle$. We obtain the following expression:

$$\hat{\varphi}(X) - \varphi_0 = \frac{\text{Re} \left[(\mathcal{T} \eta_F)^{-1/2} \langle \tilde{E}^{\text{in}} | (\partial_\varphi r)^\dagger | X \rangle - (\eta_i / \eta_F)^{1/2} \langle \tilde{E}^{\text{in}} | (\partial_\varphi r)^\dagger r | \tilde{E}^{\text{in}} \rangle \right]}{\langle \tilde{E}^{\text{in}} | (\partial_\varphi r)^\dagger \partial_\varphi r | \tilde{E}^{\text{in}} \rangle}. \quad (\text{S34})$$

Evaluating this estimator using measured data X directly yields the estimates shown in the manuscript. Note that all experimental parameters involved in this expression (i.e. \mathcal{T} , η_i and η_F) are characterized using independent measurements.

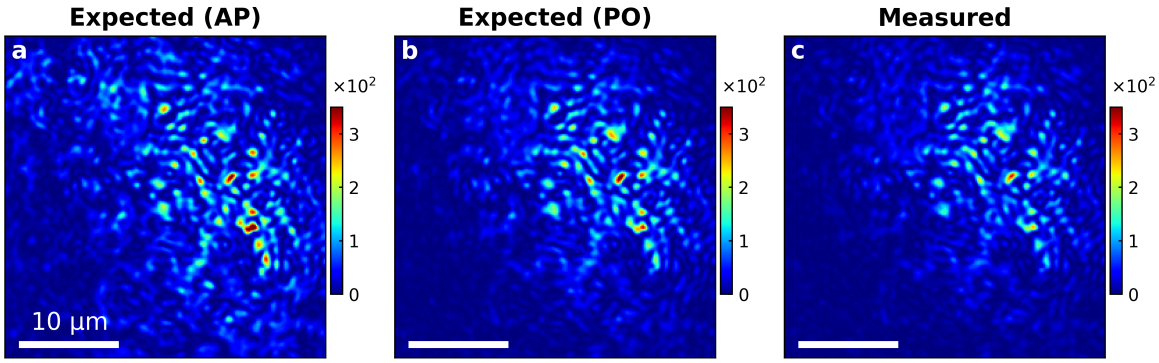
SUPPLEMENTARY SECTION S3 – CHARACTERIZATION OF THE OUTGOING FIELD AND ITS DERIVATIVE

In this section, we show that reflection matrix measurements allow to faithfully predict the outgoing field and its derivative with respect to the phase shift induced by the hidden object, and we characterize the correlation between the outgoing field distribution and its derivative.

S3.1 – Predicting the outgoing field

In general, the injection of an arbitrary state E^{in} requires amplitude-and-phase modulation of the incident field state. However, in the experiment, only the phase of the field can be modulated by the input SLM. We must therefore determine the expression of the phase-only modulated state \tilde{E}^{in} that is injected instead of E^{in} . Let us define the SLM pattern $P_{\text{SLM}} = M E^{\text{in}}$, where M is a transformation matrix mapping incident states to SLM patterns. The phase-only modulated state can be numerically approximated by $\tilde{E}^{\text{in}} = \text{argmin}(\|\tilde{P}_{\text{SLM}} - M E^{\text{in}}\|, E^{\text{in}})$, where \tilde{P}_{SLM} is the SLM pattern that has the same phase as P_{SLM} but with uniform amplitude. Thus, predicted outgoing states are given by $E_{\text{ap}}^{\text{out}} = r E^{\text{in}}$ for an amplitude-and-phase modulation, and by $E_{\text{po}}^{\text{out}} = r \tilde{E}^{\text{in}}$ for a phase-only modulation.

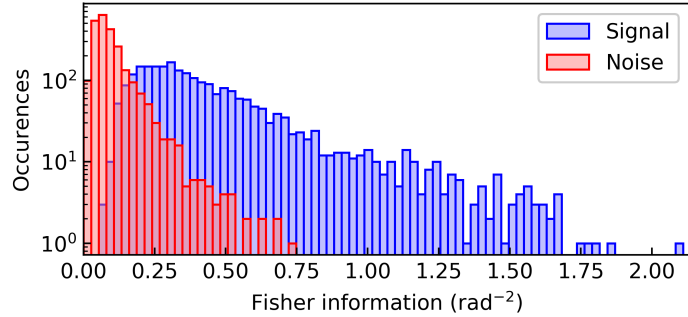
We can test this procedure by measuring the outgoing field when the optimal incident state is injected in the medium. This characterization is experimentally performed by averaging the outgoing field over 10 measurements, with the neutral density filter ND2 placed in the signal path (measured fractional transmittance $\mathcal{T}' = 0.76 \times 10^{-2}$) to avoid saturation of the camera. The complex correlation coefficient between measured and predicted fields is $0.90 + 0i$ (assuming amplitude-and-phase modulation) and $0.96 - 0.05i$ (assuming phase-only modulation). These values show that we can correctly predict the outgoing states from the measured reflection matrix. Comparing the spatial distribution of the measured intensity (Fig. S2c) to the predicted one for amplitude-and-phase modulation (Fig. S2a) and for phase-only modulation (Fig. S2b), we can see that these three distributions are indeed very similar. However, due to the presence of noise in reflection matrix measurements, we observe that the total measured intensity is lower by a factor $\eta_i = 0.84$ when compared to the predicted intensity for phase-only modulation.



Supplementary Figure S2 | Predicted and measured intensity distributions. **a, b**, Predicted spatial distribution of the normalized intensity for amplitude-and-phase (AP) modulation and phase-only (PO) modulation. **c**, Measured spatial distribution of the normalized intensity.

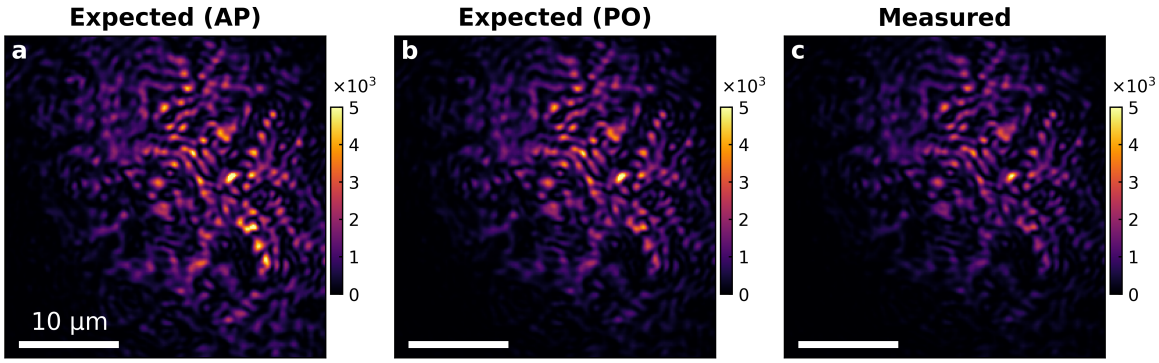
S3.2 – Predicting the derivative of the outgoing field

In order to faithfully assess the Fisher information in the experiment, we must ensure that $\partial_\varphi r$ is correctly estimated using the finite-difference scheme $\partial_\varphi r \simeq [r(\varphi_0 + \Delta\varphi) - r(\varphi_0 - \Delta\varphi)]/(2\Delta\varphi)$. To this end, the change in the measured outgoing states generated by phase variations of ± 0.54 rad must be larger than the level of noise in the measurements. In Fig. S3, we show the distribution of estimated Fisher information for each incident plane wave used to generate the reflection matrix (blue histogram). For comparison purpose, we show the distribution of noise estimates (red histogram), obtained for each plane wave by taking two identical measurements of the outgoing state for $\varphi = \varphi_0$. We clearly observe that the signal is significantly larger than the noise, with a signal mean value of 0.44 rad^{-2} and a noise mean value of 0.10 rad^{-2} .



Supplementary Figure S3 | Histograms of Fisher information and measurement noise. Histogram of Fisher information for the 2437 plane waves used to construct the reflection matrix, along with the histogram of associated measurement noise.

We can verify that this signal-to-noise ratio is sufficient to faithfully estimate $\partial_\varphi r$ by measuring the derivative of the outgoing field when the optimal incident state is injected in the medium, and comparing it to the derivative of the field predicted using $\partial_\varphi r$. This characterization is experimentally performed by averaging the outgoing field over 10 measurements, with ND2 in the signal path to avoid saturation of the camera. The complex correlation coefficient between the measured and predicted derivative of the field is $0.97 - 0.08 i$ (assuming amplitude-and-phase modulation) and $0.98 - 0.09 i$ (assuming phase-only modulation). These values show that we can correctly predict the derivative of the outgoing field from reflection matrix measurements. Comparing the spatial distribution of the measured Fisher information per unit area (Fig. S4c) to the predicted one for amplitude-and-phase modulation (Fig. S4a) and for phase-only modulation (Fig. S4b), we can see that these three distributions are very similar. However, the total measured Fisher information is lower by a factor $\eta_F = 0.80$ when compared to the predicted Fisher information for phase-only modulation. This difference is largely explained by the observed difference in the predicted and measured outgoing intensity (for which a factor $\eta_I = 0.84$ was measured).



Supplementary Figure S4 | Predicted and measured Fisher information distributions per unit area. **a, b**, Predicted spatial distribution of the normalized Fisher information per unit area for amplitude-and-phase (AP) modulation and phase-only (PO) modulation. **c**, Measured spatial distribution of the normalized Fisher information per unit area.

S3.3 – Correlation between the outgoing field state and its derivative

In order to characterize the correlation between E^{out} and $\partial_\varphi E^{\text{out}}$, we calculate the following complex correlation coefficient:

$$\mathcal{C}(E^{\text{out}}, \partial_\varphi E^{\text{out}}) = \frac{\langle E^{\text{out}} | \partial_\varphi E^{\text{out}} \rangle}{\|E^{\text{out}}\| \cdot \|\partial_\varphi E^{\text{out}}\|}. \quad (\text{S35})$$

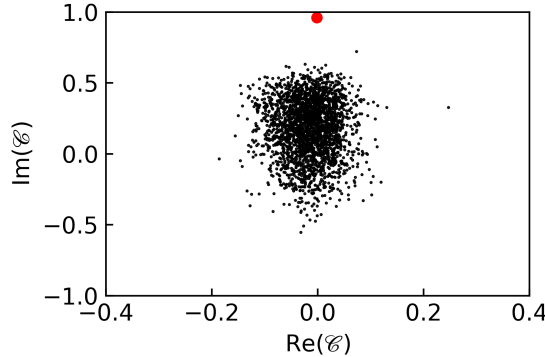
The correlation coefficient measured for plane wave illumination is on average $-0.02 + 0.18i$ (Fig. S5). For the optimal state, the measured correlation coefficient reaches $\mathcal{C} = 0.96i$, with a modulus close to unity and a negligible real part. This indicates that we can write

$$\partial_\varphi E^{\text{out}} \simeq i\gamma E^{\text{out}}, \quad (\text{S36})$$

where γ is a real coefficient. We obtain

$$E^{\text{out}}(\varphi_0 + \Delta\varphi) \simeq e^{i\gamma\Delta\varphi} E^{\text{out}}(\varphi_0). \quad (\text{S37})$$

This expression shows that the outgoing field state is invariant (to first order) with respect to a change in the parameter φ apart for a global phase shift, in the same way that principal modes of a multimode waveguide are invariant with respect to the frequency of the incident light [7–9]. While this property is characteristic of optimal states for a unitary S -matrix, it is also observed in our experiment even though the measured reflection matrix is not unitary. This



Supplementary Figure S5 | Correlation coefficient between the outgoing field and its derivative. Complex correlation coefficient between the outgoing field and its derivative for the 4273 plane waves used to construct the reflection matrix. The value of the complex correlation coefficient for the optimal incident state is represented by a red point.

observation raises the interesting question of the effect of incomplete channel control on the properties of maximum information states, which could be addressed in future work.

- [1] Kay, S. *Fundamentals of Statistical Processing, Volume I: Estimation Theory* (Prentice Hall, 1993).
- [2] Helstrom, C. W. Quantum detection and estimation theory. *J. Stat. Phys.* **1**, 231–252 (1969).
- [3] Braunstein, S. L., Caves, C. M. & Milburn, G. J. Generalized Uncertainty Relations: Theory, Examples, and Lorentz Invariance. *Ann. Phys. (N. Y.)* **247**, 135–173 (1996).
- [4] Demkowicz-Dobrzański, R., Jarzyna, M. & Kołodyński, J. Chapter Four - Quantum Limits in Optical Interferometry. In *Progress in Optics*, vol. 60, 345–435 (Elsevier, 2015).
- [5] Mandel, L. & Wolf, E. *Optical Coherence and Quantum Optics* (Cambridge University Press, 1995).
- [6] Ambichl, P. *et al.* Focusing inside Disordered Media with the Generalized Wigner-Smith Operator. *Phys. Rev. Lett.* **119**, 033903 (2017).
- [7] Fan, S. & Kahn, J. M. Principal modes in multimode waveguides. *Opt. Lett.* **30**, 135–137 (2005).
- [8] Carpenter, J., Eggleton, B. J. & Schröder, J. Observation of Eisenbud–Wigner–Smith states as principal modes in multimode fibre. *Nat. Photonics* **9**, 751–757 (2015).
- [9] Xiong, W. *et al.* Spatiotemporal Control of Light Transmission through a Multimode Fiber with Strong Mode Coupling. *Phys. Rev. Lett.* **117**, 053901 (2016).